STABILITY EVALUATION OF A LARGE-SCALE OFFSHORE WIND FARM INTEGRATED INTO A POWER SYSTEM VIA AN HVDC LINK AND AN HVAC LINE

Quang Son Vo[1*], Thanh Bac Le[2]

[1]*The University of Danang - University of Science and Technology*
[2]*The University of Danang*

*Corresponding author: vqson@dut.udn.vn

(Received: April 28, 2022; Accepted: June 13, 2022)

Abstract - Nowadays, offshore wind farms (OWFs) have been increasingly developed in many countries. This paper presents the comparative dynamic-stability evaluation of a large-scale OWF integrated into an onshore multi-machine power system via an HVDC link based on line-commutated converters (LCCs) and a high-voltage alternating current (HVAC) line. Both eigenvalue analysis based on a linearized model and time-domain simulations based on a nonlinear model of the studied system are carried out to compare the damping characteristics contributed by the LCC-HVDC link and the HVAC line. The comparative simulation results show that the LCC-HVDC link can provide better damping characteristics to stabilize the studied large-scale OWF integrated into an onshore multi-machine power system under disturbance conditions, particularly in cases of long-distance.

Key words - Eigenvalues; high-voltage direct current; offshore wind farm; stability; time-domain simulations

1. Introduction

Due to the rapid growth of global energy consumption and the environmental concerns, renewable energy sources have been increasingly implemented worldwide during the last few decades. Among the renewable sources such as wind, solar, wave, etc., wind power can be considered as one of the fastest penetrating renewable sources in power systems [1]. In addition to traditional onshore wind farms, OWFs have been increasingly developed in many countries in recent years. Currently, modern offshore wind turbines are getting bigger for meeting fundamental economic benefits. The OWFs also tend to be planned in larger capacities and further away from shore because of several convenient conditions such as strong and stable wind speed, greater space available for offshore locations, and fewer planning restrictions on OWF [2-4]. However, the integration of a large-capacity OWF over a long distance to an onshore grid can face several technical challenges such as large power fluctuations, power quality issues, stability problems, etc. [5].

To overcome the above-mentioned challenges, an HVDC link can be an attractive solution for transmitting power from a large-capacity OWF to an onshore grid because of its high-power control capability and fast-modulation ability [6], [7]. Today, although a new HVDC technology based on voltage-source converters (VSCs) has been developed, most commercial-operated HVDC systems are based on LCCs [8], [9]. The LCC-HVDC technology is particularly feasible for transmitting large amounts of electric power at very high voltages [10]. The investigations of LCC-HVDC and VSC-HVDC systems for grid-integration of large-scale OWFs have been reported in many literatures. The technical-economic analyses of HVDC transmission solutions for offshore wind power were performed in [11], [12]. Different control strategies for integrating a large-scale OWF to an onshore power grid through an LCC-HVDC link or a VSC-HVDC link were proposed in several papers [13-17]. The dynamic stability analyses of large-scale OWFs with an HVDC transmission were presented in [18-20]. In reference [21], the comparative transient-stability analysis of a permanent magnet synchronous generator (PMSG)-based OWF connected to an onshore grid through a VSC-HVDC system and an HVAC was carried out, in which the onshore grid was represented by an infinite bus.

In this paper, the stability evaluation of a large-scale doubly-fed induction generator (DFIG)-based OWF feeding power to an onshore multi-machine power system through an LCC-HVDC link and an HVAC line is presented. Both eigenvalue analysis and time-domain simulations under disturbance conditions are performed. The main contribution of this paper is to compare the damping characteristics contributed by the LCC-HVDC link and the HVAC line on stability performance of a large-scale DFIG-based OWF integrated into a multi-machine power system.

2. System configuration and mathematical models

2.1. Configuration of the studied system

Figure 1 shows the configuration of the studied 200-MW DFIG-based OWF integrated into a multi-machine power system through a 100km long LCC-HVDC link. The studied OWF is represented by a single aggregated DFIG driven by an aggregated wind turbine (WT) through an aggregated gearbox (GB). The OWF is connected to the LCC-HVDC link through a step-up transformer and a connection cable. The LCC-HVDC link comprising an LCC-rectifier, a T-equivalent direct-current (DC) transmission line, and an LCC-inverter transmit the generated power from the OWF to Bus #5 of the multi-machine power system. The capacitors C_R and C_I at Bus #15 and Bus #16 represent the capacitor banks used to provide reactive power for the operation of the LCC-HVDC link, respectively. When performing the analysis of an HVAC line for connecting the studied OWF to Bus #5, the LCC-HVDC link in Figure 1 will be replaced by an HVAC line. The studied multi-machine power system

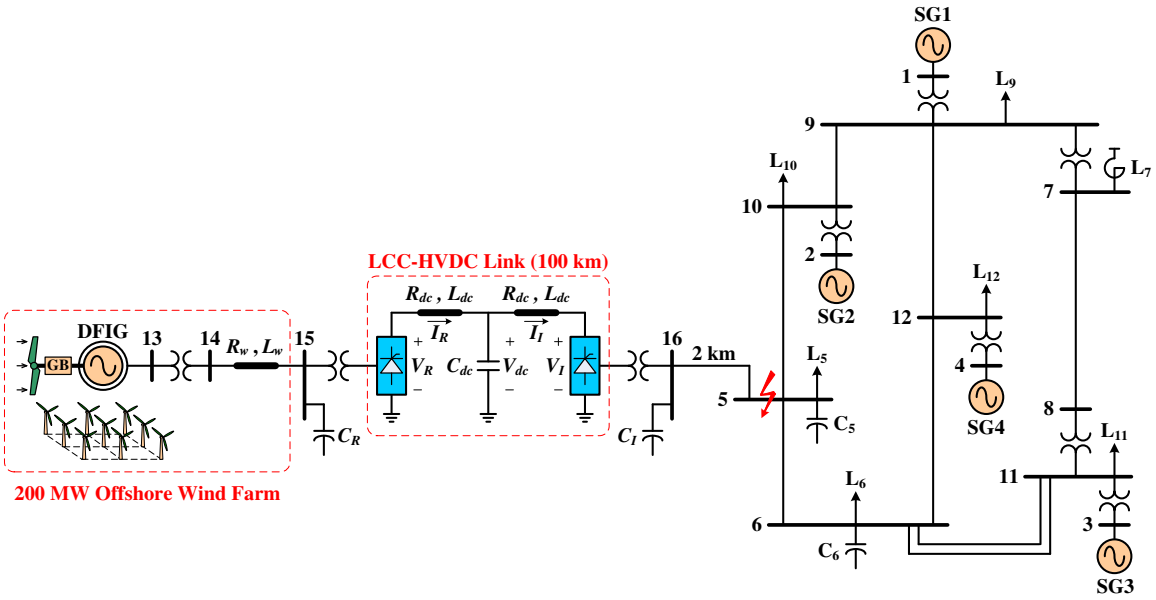

Figure 1. *Configuration of the studied OWF integrated into a multi-machine power system through an LCC-HVDC link*

shown on the right side of Figure 1 is the generic 12-bus power system [22] which consists of four synchronous generators (SGs), loads, and the interconnected transmission network mainly at 230 kV level. The employed mathematical models for the subsystems shown in Figure 1 are described hereafter.

2.2. DFIG-based OWF model

The studied 200-MW DFIG-based OWF is modeled as a single aggregated DFIG-based wind power generation system (WPGS). The fundamental configuration of a DFIG-based WPGS is that the stator windings of the DFIG are directly connected to the grid. The rotor windings of the DFIG are connected to the same grid through a rotor-side converter, a DC link, and a grid-side converter (GSC). The DFIG is driven by a WT that is mechanically coupled to the rotor of the DFIG through a mechanical drive train system. More detailed descriptions and employed mathematical equations for various components of the DFIG-based WPGS including controllers are referred to reference [23].

2.3. LCC-HVDC link model

The LCC-HVDC link model consists of a rectifier, a DC transmission line, and an inverter [24]. The per-unit (pu) DC voltages of the rectifier V_R and the inverter V_I can be expressed by [24], respectively:

$$V_R = k_R V_{SR} \cos(\alpha_R) - (\pi/6) X_{CR} I_R \quad (1)$$

$$V_I = k_I V_{SI} \cos(\gamma_I) - (\pi/6) X_{CI} I_I \quad (2)$$

where V_{SR} and V_{SI} are the AC voltages (in pu) of the rectifier and the inverter, respectively; α_R is the firing angle of the rectifier (in degree) and γ_I is the extinction angle of the inverter (in degree); I_R and I_I are the DC currents (in pu) of the rectifier and the inverter, respectively; X_{CR} and X_{CI} are the commutation reactances (in pu) of the rectifier and the inverter, respectively; k_R and k_I are unity in pu system.

The DC transmission line, as shown in Figure 1, is represented by a T-equivalent circuit whose pu dynamic equations can be obtained as

$$(L_{dc}/\omega_b)\, p(I_R) = V_R - R_{dc} I_R - V_{dc} \quad (3)$$

$$(C_{dc}/\omega_b)\, p(V_{dc}) = I_R - I_I \quad (4)$$

$$(L_{dc}/\omega_b)\, p(I_I) = V_{dc} - R_{dc} I_I - V_I \quad (5)$$

where p is the differential operator with respect to time t ($p = d/dt$); ω_b is the base angular frequency (in rad/s) R_{dc}, L_{dc}, and C_{dc} and the resistance, inductance, and capacitance of the DC transmission line model, respectively; and V_{dc} is the voltage on the capacitance C_{dc}.

Figure 2 shows the control-block diagrams for the rectifier and the inverter of the LCC-HVDC link. The rectifier's current I_R is controlled through adjusting the firing angle α_R of the rectifier by using the control-block diagram for the rectifier as shown in Figure 2(a). On the other hand, the inverter current I_I can be regulated through altering the extinction angle γ_I of the inverter by employing the control-block diagram for the inverter as depicted in Figure 2(b) [18], [24].

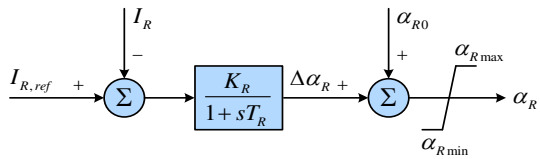

(a) Control-block diagram for the rectifier

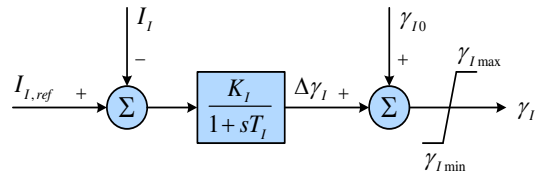

(b) Control-block diagram for the inverter

Figure 2. *Control block diagrams for the rectifier and the inverter of the LCC-HVDC link*

2.4. Multi-machine power system model

As mentioned earlier, the studied multi-machine power system is the 12-bus power system [22] consisting of four SGs, loads, and the interconnected transmission network. The SGs are modeled by employing the two-axis model of a SG. The pu differential equations for the *i*-th SG are given by [25]

$$\left(T'_{qoi}\right) p\left(E'_{di}\right) = -E'_{di} + \left(X_{qi} - X'_{qi}\right) I_{qi} \tag{6}$$

$$\left(T'_{doi}\right) p\left(E'_{qi}\right) = -E'_{qi} - \left(X_{di} - X'_{di}\right) I_{di} + E_{fdi} \tag{7}$$

$$\left(2H_i\right) p\left(\omega_i\right) = T_{mi} - E'_{di} I_{di} - E'_{qi} I_{qi} - \left(X'_{qi} - X'_{di}\right) I_{di} I_{qi} - D_i\left(\omega_i - 1\right) \tag{8}$$

$$p\left(\delta_i\right) = \omega_b\left(\omega_i - 1\right) \tag{9}$$

where the subscript *i* denotes the quantities of the *i*-th SG, E'_{di} and E'_{qi} are the *d*- and *q*-axis voltages behind transient impedance, respectively; ω_i is the rotor speed; δ_i is the rotor angle (in rad); I_{di} and I_{qi} are the *d*- and *q*-axis stator currents, respectively; E_{fdi} is the field voltage; T'_{doi} and T'_{qoi} are the *d*- and *q*-axis transient open-circuit time constants (in s), respectively; X_{di} and X_{qi} are the *d*- and *q*-axis synchronous reactances, respectively; X'_{di} and X'_{qi} are the *d*- and *q*-axis transient reactances, respectively; T_{mi} is the mechanical torque; H_i is the inertia constant (in s); D_i is the damping coefficient.

The loads at different buses are modeled as constant impedances while the transients associated with the transmission network of the 12-bus power system are neglected. Under these assumptions, the transmission network the 12-bus power system can be simply represented by its bus admittance matrix Y_{BUS} [26].

The complete parameters, the DFIG-based OWF and the 12-bus power system can be referred to references [23] and [22], respectively, while the employed parameters of the LCC-HVDC link with its controllers are listed in Table 1 below.

Table 1. *Parameters of the LCC-HVDC link with its controllers*

Ratings	P_{rated} = 200 MW, $V_{dc,rated}$ = 160 kV
Capacitor banks	C_R = 0.6 pu, C_I = 0.6 pu
Commutation reactances	X_{CR} = 0.051 pu, X_{CI} = 0.051 pu
DC line	R_{dc} = 0.004 pu, L_{dc} = 0.178 pu, C_{dc} = 12.5 pu
Rectifier controller	K_α = 1.0, T_α = 0.1 s, α_{R0} = 17°
Inverter controller	K_γ = 1.0, T_γ = 0.1 s, γ_{I0} = 17°

3. Eigenvalue and root-loci analysis

Eigenvalue analysis [26] is one of the most widely used methods to evaluate the small-signal stability of power systems. The stability margin of a power system under different operating conditions can also be observed by tracking the root-loci of its eigenvalues. In this section, the comparative eigenvalue analyzed results of the studied system with the LCC-HVDC link and the HVAC line are presented. The comparative root-loci of the system eigenvalues under different lengths of the transmission systems are also examined. The steps to obtain the system eigenvalues are as follows: (i) The nonlinear system model developed in the previous section is linearized around an operating point to obtain the corresponding linearized system model which is a set of linearized equations in a matrix form and (ii) the numerical calculations of the system state matrix **A** of the linearized system model and its associated eigenvalues are carried out by using MATLAB program.

3.1. System eigenvalues analysis

Table 2 lists the comparative dominant eigenvalues of the studied DFIG-based OWF integrated to the 12-bus power system through the LCC-HVDC link and the HVAC line under a selected operating point in which the wind speed of the OWF is 11 m/s and the operating conditions of the 12-bus power system are assumed to be the same as ones specified in [22]. Other eigenvalues which are located far away from the imaginary-axis on the left-hand side of the complex plane have been neglected. A participation factor analysis [26] has been performed to identify the state variables participating in each eigenvalue and thus the corresponding mode of each eigenvalue. As illustrated in Table 2, the eigenvalues Λ_1 to Λ_6 are identified as the electromechanical modes relating to the electromechanical interactions among the SGs of the 12-bus power system. The eigenvalues $\Lambda_{7,8}$ and $\Lambda_{9,10}$ are a control mode and the electromechanical mode of the DFIG-based OWF, respectively.

Table 2. *Dominant eigenvalues (rad/s) [damping ratio/ frequency (Hz)] of the studied system under the OWF's wind speed V_w of 11 m/s*

Eigen-value	Sub-system	Mode	System with an HVAC line	System with an LCC-HVDC link
$\Lambda_{1,2}$	12-bus power system	Electro-mechanical modes	-4.367 ± *j*9.023 [0.436/1.436]	-4.439 ± *j*9.126 [0.437/1.452]
$\Lambda_{3,4}$			-2.725 ± *j*8.825 [0.295/1.404]	-2.760 ± *j*8.849 [0.298/1.408]
$\Lambda_{5,6}$			-1.270 ± *j*7.400 [0.169/1.178]	-1.313 ± *j*7.374 [0.175/1.174]
$\Lambda_{7,8}$	DFIG-based OWF	Control mode	-0.498 ± *j*4.041 [0.122/0.643]	-0.806, -0.573 [1.0/--]
$\Lambda_{9,10}$		Electro-mechanical mode	-1.944 ± *j*26.339 [0.074/4.192]	-2.281 ± *j*41.947 [0.054/6.676]

Comparing the dominant eigenvalues listed in the last two columns of Table 2, it is clearly seen that the dominant modes of the 12-bus power system are very similar in both cases while the dominant modes of the DFIG-based OWF are significantly different. It is found that the complex-conjugated eigenvalues $\Lambda_{7,8}$ denoting oscillatory modes in the studied system with the HVAC line have been separated into two negative real eigenvalues relating to non-oscillatory modes in the studied system with the LCC-HVDC link. Moreover, the complex-conjugated eigenvalues $\Lambda_{9,10}$ in the studied system with the LLC-HVDC link have located further into the left-half of the complex plane and they have higher oscillating frequencies when compared with the ones in the studied system with the HVAC line. Therefore, it can be concluded from the

comparative dominant eigenvalues listed in Table 2 that the LCC-HVDC link can contribute better damping characteristics to the oscillatory modes of the DFIG-based OWF than the HVAC line. However, their damping effects on the onshore power grid represented by the 12-bus power system are almost identical.

3.2. Root-loci analysis

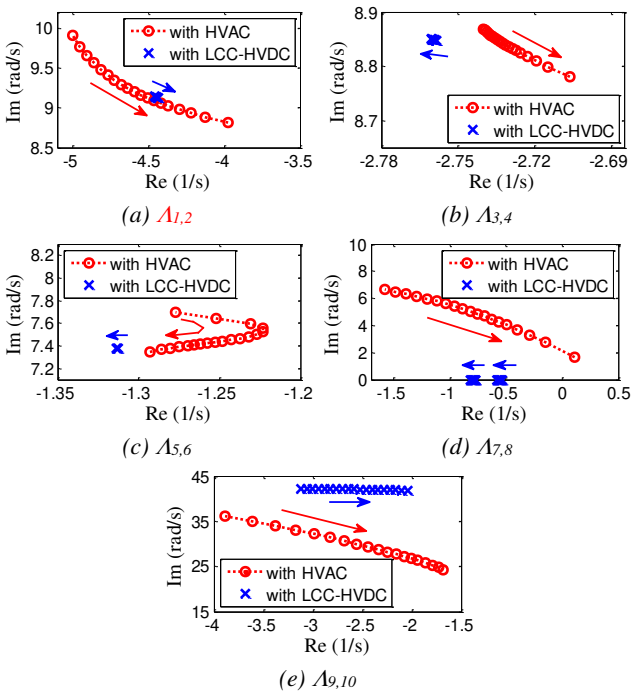

Figure 3. *Root-loci of the system dominant eigenvalues under the variations of the length of the LCC-HVDC link and the HVAC line*

In this sub-section, the sensitivity analysis of the system dominant modes on variations of the length of the alternative LCC-HVDC link and HVAC line is presented. Since nowadays OWFs tend to be planned further from shore, the purpose of this study is to compare the damping effects contributed by the alternative LCC-HVDC link and HVAC line when the studied DFIG-based OWF is assumed to be located at different distances from the onshore power grid. Figure 3 plots the comparative root-loci results for the system dominant modes when the length of the LCC-HVDC link and HVAC line is increased from 30 km to 120 km. The arrows shown in Figure 3 indicate the directions of the root-loci when the length of the LCC-HVDC link and the HVAC line is increased. It is clearly seen from the root-loci results shown in Figure 3 that the studied system with a short HVAC line is quite stable since all the system dominant modes locates far from the imaginary axis on the left-hand side of the complex plane. However, the dominant modes are very sensitive to the length of the HVAC line and move rapidly to the imaginary axis as the length of the HVAC line is increased. The most noticeable case is observed when the length of HVAC line reaches 120 km. In such a case, the mode $\Lambda_{7,8}$ has moved to the right-hand side of the complex plane which indicates an unstable system. On the contrary, the dominant modes of the studied system with the LCC-HVDC link are much less sensitive to the length of the LCC-HVDC link since they are almost fixed on the left-hand side of the complex plane regardless the increasing of the length of the LCC-HVDC link. Therefore, the root-loci results plotted in Figure 3 have demonstrated that the LCC-HVDC link is superior to the HVAC line for integrating the OWFs located far-offshore.

4. Time-domain simulations

This section employs the nonlinear-system model developed in Section 2 to compare the transient responses of the studied DFIG-based OWF integrated to the 12-bus power system through the LCC-HVDC link and the HVAC line subject to a severe disturbance. A three-phase short-circuit fault lasting for 5 cycles (0.083 s) is suddenly applied to Bus #5 at t = 1.0 s. The comparative transient responses are shown in Figure 4. The dashed-red lines in Figure 4 represent the transient responses of the studied system with the HVAC line while the solid-blue lines in Figure 4 represent the ones of the studied system with the LCC-HVDC link.

Figure 4(a)-(d) depicts the comparative transient responses of the rotor speed of the four SGs. It can be found in these results that the transient responses of these quantities are similar in both cases although there have been slightly better damping characteristics in the transient responses of the studied system with the LCC-HVDC link. Therefore, the difference in damping effects contributed by the HVAC line and the LCC-HVDC link to the transient responses of the 12-bus power system are insignificant. These results agree well with the eigenvalue analyzed results presented in the previous section.

The transient responses of the quantities of the studied DFIG-based OWF such as terminal voltage V_{DFIG}, active power P_{DFIG}, and rotor speed ω_{DFIG} are shown in Figure 4(e)-(g). When the studied DFIG-based OWF is fed through the HVAC line, it is seen from the transient responses shown in Figure 4(e)-(f) that the fault at Bus #5 causes the output voltage and active power of the DFIG to be dropped considerably. Since the wind speed is assumed to be constant during the fault, the mechanical input power applied to the WT is still as high as that in the pre-fault condition. Therefore, the large imbalance between the input and output power will result in the rotor speed of the DFIG accelerating rapidly during the fault, as can be observed in Figure 4(g). In the case of the studied system with the LCC-HVDC link, during the fault, the control system of the LCC-HVDC link will act to regulate the increasing DC current back to its reference value. Consequently, the output voltage and active power of the DFIG can be suppressed from a significant drop, as depicted in Figure 4(e)-(f). It is also obviously seen in Figure 4(g) that the rotor speed of the DFIG in this case is just slightly increased. At the instant of the fault being cleared, the oscillations will be excited in both cases of the studied system. It can be clearly seen that the oscillations in the transient responses of the studied system with the LCC-HVDC link can be quickly damped out after 1.0 s while the oscillations in the responses of the studied system with the HVAC line still oscillate after 4.0 s. In other words, since the LCC-HVDC link has the control system

which will act to regulate the DC line current during the fault, it can render better damping characteristics to damp out the oscillations of the DFIG-based OWF fed to the multi-machine power system than the HVAC line.

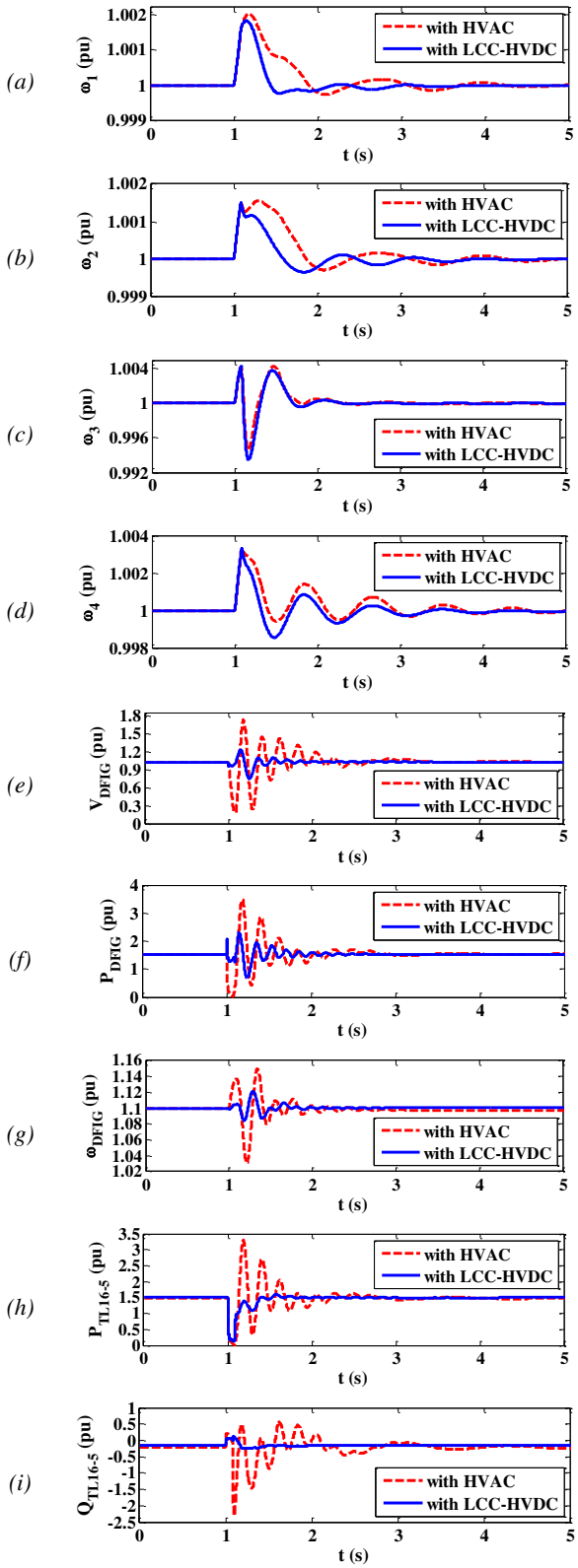

Figure 4. *Comparative transient responses of the studied system subject to a three-phase short-circuit fault at Bus #5: (a) ω_1, (b) ω_2, (c) ω_3, (d) ω_4, (e) V_{DFIG}, (f) P_{DFIG}, (g) ω_{DFIG}, (h) $P_{TL16\text{-}5}$, (i) $Q_{TL16\text{-}5}$*

Figure 4(h)-(i) illustrates the comparative transient responses of the active and reactive powers from the OWF fed to Bus #5, respectively. These responses demonstrate that the LCC-HVDC link can smooth the electrical power of the OWF delivered to the 12-bus power system better than the HVAC line under the applied three-phase short-circuit fault condition at Bus #5.

To verify the root-loci analysis results presented in previous section, further time-domain simulations of the studied system with three different cases of the length of the LCC-HVDC link and the HVAC line, i.e., 80 km, 100 km, and 120 km, have been conducted. The same three-phase short-circuit fault as above is applied in each case of simulation. Figure 5 plots the transient responses of the active power from the OWF fed to Bus #5 resulting from the three simulation cases. It can be clearly found from the transient responses shown in Figure 5 that the studied system with the LCC-HVDC link is very stable in all three cases while the stability of the studied system with the HVAC line deteriorates significantly as the length of the HVAC line is increased. The instability case is revealed in the third plot when the length of the HVAC line is 120 km. These results agree well with the root-loci analysis results shown in the previous section.

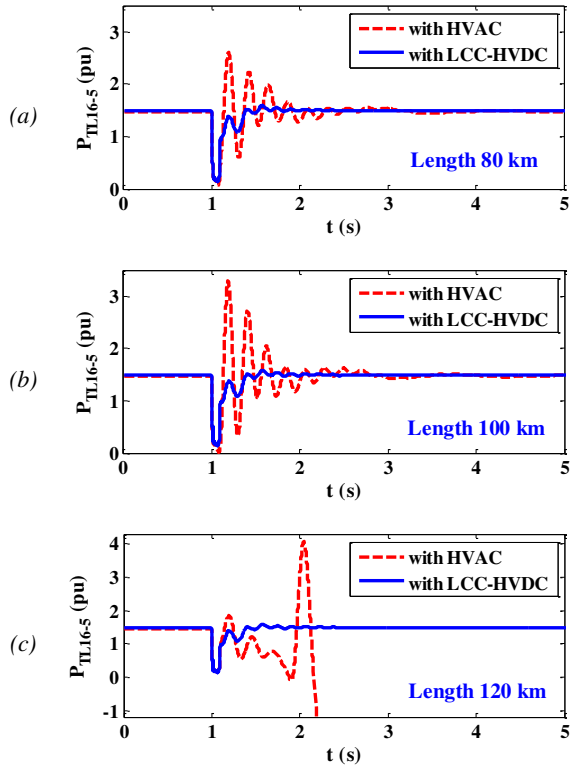

Figure 5. *Transient responses of the active power from the OWF fed to Bus #5 in three cases of length of the LCC-HVDC link and HVAC line: (a) 80 km, (b) 100 km, (c) 120 km*

5. Conclusions

This paper has presented the comparative dynamic-stability evaluation of a 200-MW DFIG-based OWF integrated into a multi-machine power system through an LCC-HVDC link and an HVAC line. The eigenvalue technique has been employed to compare the damping

characteristics contributed by the LCC-HVDC link and the HVAC line. The comparative transient responses of the studied system subject to a severe three-phase short-circuit fault at the integration bus have been carried out by using the nonlinear system model simulations. Through the comparative eigenvalue and transient response analyzed results, the following conclusions can be figured out:

(i) The LCC-HVDC link can provide better damping characteristics to stabilize the studied 200-MW DFIG-based OWF fed to the multi-machine power system subject to a severe fault than the HVAC line. The reason for this is that the LCC-HVDC link has the controller system which can regulate the DC line current during the fault, whereas the HVAC line does not have the control capability to regulate the current flow through it.

(ii) If there is no additional control solution for the HVAC line (for example using FACTS devices), the HVAC line might not be employed for integrating the studied 200-MW DFIG-based OWF to the onshore grid when the transmission distance is larger than 120 km since the simulation results revealed that the studied system is unstable at the examined operating point in such the case.

(iii) If studied DFIG-based OWF is located not very far from the shore, the short-length HVAC line will not degrade stability of the studied system significantly. In that case, the LCC-HVDC link might not be clearly superior to the HVAC line. Hence, the HVAC line can be selected over the LCC-HVDC link for integrating the OWFs with short-distances to the onshore grid due to its simple structure and low installation cost.

REFERENCES

[1] P. O. Dorile, D. R. Jagessar, L. Guardado, R. A. McCann, and M. Ahanch, "Grid strength assessment and maximum loadability of a wind-dominated power system through QV modal analysis", in *Proc. 2021 IEEE PES/IAS PowerAfrica*, 2021, pp. 1-5.

[2] B. Yang *et al.*, "A critical survey of technologies of large offshore wind farm integration: summary, advances, and perspectives", *Protection and Control of Modern Power Systems*, vol. 7, no. 17, pp. 1-32, May 2022.

[3] C. Li, P. Zhan, J. Wen, M. Yao, N. Li, and W.-J. Lee, "Offshore wind farm integration and frequency support control utilizing hybrid multiterminal HVDC transmission", *IEEE Trans. Industry Applications*, vol. 50, no. 4, pp. 2788-2797, Jul./Aug. 2014.

[4] S. Chuangpishit, A. Tabesh, Z. Moradi-Shahrbabak, and M. Saeedifard, "Topology design for collector systems of offshore wind farms with pure dc power systems", *IEEE Trans. Industrial Electronics*, vol. 61, no. 1, pp. 320-328, Jan. 2014.

[5] S. W. Ali *et al.*, "Offshore wind farm-grid integration: A review on infrastructure, challenges, and grid solutions", *IEEE Access*, vol. 9, pp. 102811-102827, Jul. 2021.

[6] R. E. Torres-Olguin, M. Molinas, and T. Undeland, "Hybrid HVDC connection of large offshore wind farms to the ac grid", in *Proc. 2012 IEEE Int. Symp. Industrial Electronics (ISIE)*, pp. 1591-1597.

[7] N. M. Kirby, L. Xu, M. Luckett, and W. Siepmann, "HVDC transmission for large offshore wind farms", *Power Engineering Journal*, vol. 16, no. 3, pp. 135-141, Jun. 2002.

[8] S. Cole and R. Belmans, "Transmission of bulk power", *IEEE Industrial Electronics Magazine*, vol. 3, no. 3, pp. 19-24, Sep. 2009.

[9] M. Daryabak et al., "Modeling of LCC-HVDC systems using dynamic phasors", *IEEE Trans. Power Delivery*, vol. 29, no. 4, pp. 1989-1998, Aug. 2014.

[10] L. Weimers, "Bulk power transmission at ±800 kV dc", ABB Power Technologies, Ludvika, Sweden. [Online]. Available: www.abb.com

[11] B. V. Eeckhout1, D. V. Hertem, M. Reza, K. Srivastava, and R. Belmans, "Economic comparison of VSC HVDC and HVAC as transmission system for a 300MW offshore wind farm", *Euro. Trans. Electrical Power*, vol. 20, no. 5, pp. 661-671, Jul. 2010.

[12] P. Bresesti, W. L. Kling, R. L. Hendriks, and R. Vailati, "HVDC connection of offshore wind farms to the transmission system", *IEEE Trans. Energy Conversion*, vol. 22, no. 1, pp. 37-43, Mar. 2007.

[13] S. V. Bozhko, R. Blasco-Gimenez, R. Li, J. C. Clare, and G. M. Asher, "Control of offshore DFIG-based wind farm grid with line-commutated HVDC connection", *IEEE Trans. Energy Conversion*, vol. 22, no. 1, pp. 71-78, Mar. 2007

[14] R. Blasco-Gimenez, N. Aparicio, S. Ano-Villalba, and S. Bernal-Perez, "LCC-HVDC connection of offshore wind farms with reduced filter banks", *IEEE Trans. Industrial Electronics*, vol. 60, no. 6, pp. 2372-2380, Jun. 2013.

[15] D. Xiang, L. Ran, J. R. Bumby, P. J. Tavner, and S. Yang, "Coordinated control of an HVDC link and doubly fed induction generators in a large offshore wind farm", *IEEE Trans. Power Delivery*, vol. 21, no. 1, pp. 463-471, Jan. 2006.

[16] M. M. Kabsha and Z. H. Rather, "A new control scheme for fast frequency support from HVDC connected offshore wind farm in low-inertia system", *IEEE Trans. Sustainable Energy*, vol. 11, no. 3, pp. 1829-1937, Jul. 2020.

[17] D. Xiang, L. Ran, J. R. Bumby, P. J. Tavner, and S. Yang, "Coordinated control of an HVDC link and doubly fed induction generators in a large offshore wind farm", *IEEE Trans. Power Delivery*, vol. 21, no. 1, pp. 463-471, Jan. 2006.

[18] L. Wang and M. S.-N. Thi, "Stability analysis of four PMSG-based offshore wind farms fed to an SG-based power system through an LCC-HVDC link", *IEEE Trans. Industrial Electronics*, vol. 60, No. 6, pp. 2392-2400, Jun. 2013.

[19] L. P. Kunjumuhammed, B. C. Pal, R. Gupta, and K. J. Dyke, "Stability Analysis of a PMSG based large offshore wind farm connected to a VSC-HVDC", *IEEE Trans. Energy Conversion*, vol. 32, no. 3, pp. 1166-1176, Sep. 2017.

[20] A. Haghi and M. Rahimi, "Control and stability analysis of VSC-HVDC based transmission system connected to offshore wind farm", *Trans. Computer Science & Engineering and Electrical Engineering (D)*, vol. 29, no. 1, pp. 193-207, Jan./Feb. 2022.

[21] N. Inaba, R. Takahashi, J. Tamura, M. Kimura, A. Komura, and K. Takeda, "Transient stability analysis of HVAC or HVDC transmission system based offshore wind farm", in *Proc. 2012 15th Int. Conf. Electrical Machines and Systems (ICEMS)*, pp. 1-6.

[22] A. Adamczyk, M. Altin, O. Goksu, R. Teodorescu, and F. Iov, "Generic 12-bus test system for wind power integration studies", in *Proc. 2013 15th European Conf. Power Electronics and Applications*, pp. 1–6.

[23] L. Wang and Q.-S. Vo, "Power flow control and stability improvement of connecting an offshore wind farm to a one-machine infinite-bus system using a static synchronous series compensator", *IEEE Trans. Sustainable Energy*, vol. 4, no. 2, pp. 358-369, Mar. 2013.

[24] L. Wang, K.-H. Wang, W.-J. Lee, and Z. Chen, "Power-flow control and stability enhancement of four parallel-operated offshore wind farms using a line-commutated HVDC link", *IEEE Trans. Power Delivery*, vol. 25, no. 2, pp. 1190-1202, Apr. 2010.

[25] P. W. Sauer and M. A. Pai, *Power System Dynamics and Stability*. Upper Saddle River, NJ: Prentice-Hall, 1998.

[26] P. Kundur, *Power System Stability and Control*. New York: McGraw-Hill, 1994.